Elucidation of Spheroid Formation With and Without the Extrusion Step

Submitted: December 29, 2005; Accepted: July 19, 2006; Published: February 9, 2007

Celine V. Liew,[1] Siang Meng Chua,[1] and Paul W.S. Heng[1]

[1]Department of Pharmacy, National University of Singapore, 18 Science Drive 4, Singapore 117543, Singapore

ABSTRACT

Spheroid formation mechanisms were investigated using extrusion-spheronization (ES) and rotary processing (RP). Using ES (cross-hatch), ES (teardrop), and RP (teardrop), spheroids with similar mass median diameter (MMD) and span were produced using equivalent formulation and spheronization conditions. During spheronization, the teardrop-studded rotating frictional surface, with increased peripheral tip speed and duration, produced spheroids of equivalent MMD and span to those produced by the cross-hatch rotating frictional plate surface. The roundness of these spheroids was also similar. RP required less water to produce spheroids of MMD similar to that of spheroids produced by ES. However, these RP spheroids were less spherical. Image analysis of 625 spheroids per batch indicated that the size distribution of RP spheroids had significantly greater SD, positive skewness, and kurtosis. Morphological examination of time-sampled spheroids produced by ES indicated that spheroid formation occurred predominantly by attrition and layering, while RP spheroids were formed by nucleation, agglomeration, layering, and coalescence. RP produced spheroids with higher crushing strength than that of ES-produced spheroids. The amount of moisture lost during spheronization for spheroids produced by ES had minimal influence on their eventual size. Differences in process and formulation parameters, in addition to size distribution and observed morphological changes, enabled a greater understanding of spheroid formation and methods to optimize spheroid production.

KEYWORDS: Rotary processing, extrusion, spheronization, spheroids, formation mechanism.

INTRODUCTION

Spheronization is a process in which powders or agglomerating granules are made spherical and free-flowing. Generally, the useful size range of spheroids for pharmaceutical use is between 0.5 and 1.5 mm. Extrusion-spheronization (ES) and rotary processing (RP) are 2 more commonly recognized techniques employed for manufacturing spheroids.[1]

Corresponding Author: Paul W.S. Heng, Department of Pharmacy, National University of Singapore, 18 Science Drive 4, Singapore 117543. Tel: (65) 6516 2930; Fax: (65) 6775 2265; E-mail: phapaulh@nus.edu.sg

Both ES and RP require the powder mix to be moistened, agglomerated, and densified. ES is a multistep process, encompassing wet massing, extrusion, and spheronization.[2] During spheronization, extrudates are broken up and undergo remodeling into spheroids.[3]

Physical changes experienced by extrudates have been studied using Plasticine[4] and photography.[5] Dumbbell-shaped extrudates were observed in 20 seconds of spheronization and were hypothesized to be formed when the extrudates were compressed along the length, causing shortening and rounding at the ends.[5] On the other hand, Baert and Remon[4] proposed that extrudates experience spheronization by going through a ropelike, dumbbell-shaped intermediate before being separated into 2 spheroid precursors. Each of the precursors would then be rounded into spheroids.

In contrast to ES, RP allows liquid addition, agglomeration, and spheronization to take place as a 1-step/1-pot process.[6] Unlike in ES, in RP wet massing, agglomeration, and spheronization occur simultaneously and the interplay of these process steps results in spheroid formation.

Extensive studies have investigated the process and formulation parameters affecting ES and RP. However, reports comparing spheroid production by these 2 methods are limited. Pisek et al[7] reported that RP spheroids were of broader size distribution and higher density but were more brittle. The comparisons were made between spheroids of different mean sizes. By varying rotor speed, spray rate, and drug loading, Robinson and Hollenbeck[8] used RP to produce spheroids that had similar dissolution rates and crushing strengths as those produced by ES.

Although ES and RP are 2 different methods that use different types of equipment, they share a common feature: the rotating frictional plate. Material undergoing spheronization is subjected to frictional forces provided by a rotating frictional plate with a textured surface. The surface texture of the rotating frictional plate used in ES is often cross-hatch square pyramidal studs with rectangular grooves, while the rotating frictional plate residing in the RP product chamber is teardrop studded. A gap is present between the rotating frictional plate and the chamber wall for both the spheronizer and the rotary processor. In the rotary processor, because powder mix could be lost through the gap, pressurized air or gap air is introduced from the bottom. In the spheronizer, the starting material is extrudates of an appreciable size. Thus, gap air is not needed.

In ES studies, cross-hatch or radial-textured rotating frictional plates were found not to affect spheroid quality unless the extrudates were of poor quality.[9] RP studies indicated that the size and roundness of spheroids would be increased with an increase in the height of the teardrop protuberances on the rotating frictional plate.[10] Apart from standardizing formulation variables, equivalency in the effect of the frictional plates between ES and RP could be empirically established if extrudates, spheronized by respective cross-hatch and teardrop-studded rotating frictional plates, yielded spheroids of comparable quality. In this study, spheronization conditions such as peripheral tip speed and duration of the teardrop-studded rotating frictional plate[10,11] would be adjusted when elucidating for equivalency in effect between cross-hatch or teardrop-studded frictional plates during spheronization of extrudates on the plates. Subsequently, using standardized formulation and equivalent spheronization conditions, processing parameters for RP would be adjusted to produce spheroids of equivalent size to those of ES. Processing parameters for ES and RP would be compared to elucidate their effects on spheroid quality and the formation mechanism.

Materials and Methods

Preparation of Spheroids

A formula capable of producing good-quality spheroids by ES was chosen. Characteristics of the ES spheroids were compared with those of RP spheroids. A binary mixture of microcrystalline cellulose (MCC) (Avicel PH101, Asahi Chemical, Tokyo, Japan) and lactose monohydrate (Pharmatose 200M, De Melkindustrie Veghel, Veghel, The Netherlands) in a ratio of 1:3 was preblended using a twin cone mixer (AR401, Erweka, Heusenstamm, Germany) at 40 rpm for 1 hour.

Spheroids were produced using 3 different techniques: 1. ESC: ES with cross-hatch plate; 2. EST: ES with teardrop-studded plate; RT: RP with teardrop-studded plate (Figure 1).

For ESC and EST, wet massing of a 1-kg load of MCC: lactose powder mixture was performed in a planetary mixer (Kenwood Major, Havant, UK). Distilled water amounting to 380 mL was used as the granulating liquid and introduced at a flow rate of ~40 mL/min using a peristaltic pump (502S, Watson-Marlow, Falmouth, UK). The resultant wet mass was extruded by a radial extruder (E140, GEA-Niro, Eastleigh, UK) fitted with an extrusion screen of 1 mm aperture diameter and thickness. The extrusion feed rate and the extrusion speed were set at 60 rpm and 47 rpm, respectively. The extrudates produced were then spheronized. For ESC, a cross-hatch frictional plate was used in a spheronizer (S320, GEA-Niro, UK). For EST, spheronization was performed on a teardrop-studded frictional plate in a multisystem air handling unit (MP1, Aeromatic-Fielder, Eastleigh, UK) equipped with a rotary processor module. Details of the frictional plates are given in Table 1 and Figure 2. The selected process parameters for ESC and EST are shown in Table 2. For each batch, spheroids were sampled at half-minute intervals during spheronization for size and shape analysis. For ESC

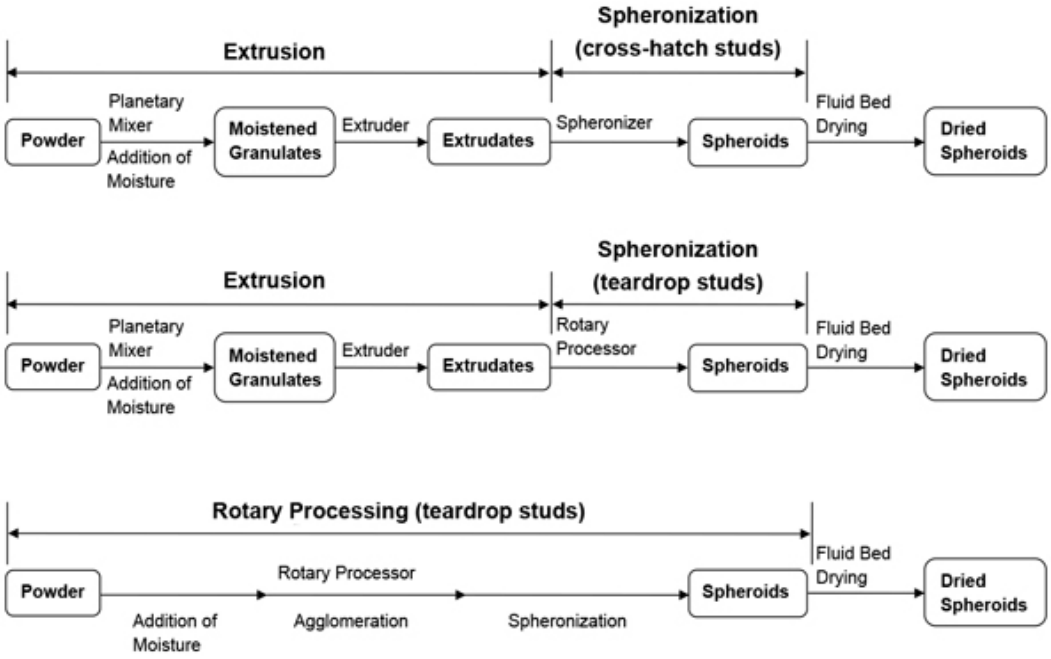

Figure 1. Schematics showing processes leading to spheroid formation.

Table 1. Details of Equipment Used for Spheronization of Extrudates*

Process	Spheronizing Equipment	Diameter of Frictional Plate (mm)	Texture of Frictional Plate
ESC	Spheronizer (S320, GEA-Niro, Eastleigh, UK)	320	Cross-hatch design plate (grooves with edges well defined and reasonably sharp)
EST	Rotary processor (MP1, Aeromatic-Fielder, Eastleigh, UK)	275	Teardrop-studded plate (stud height, 2.75 mm; edges rounded)[9]

*ESC indicates extrusion-spheronization with cross-hatch plate; EST, extrusion-spheronization with teardrop-studded plate.

spheroids, video footage of the first 2 seconds of spheronization was taken using a high-speed camera (MotionPro HS-3, Redlake, Tucson, AZ) at 1000 fps and shutter speed at 86 μs. All runs were performed in triplicate, and results were averaged. The batches were coded according to the processes used and the speed of the frictional plate.

RP was performed using the rotary processor module, coupled to a multisystem air handling unit (MP1, Aeromatic-Fielder, Eastleigh, UK). The rotating frictional plate used for RP was identical to that used for EST. A 1-kg load of the MCC/lactose binary mixture was used per batch. Three different amounts of water (360 g, 370 g, and 380 g) were used to produce spheroids by RP; batches were coded appropriately (RT36%, RT37%, and RT38%). For size and shape analysis, spheroids were sampled at half-minute intervals after completion of the water addition. The process parameters used are shown in Table 3, and runs were performed in triplicate.

Drying of Spheroids

The spheroids produced were dried in a fluid bed dryer (Strea-1, GEA-Aeromatic, Bubendorf, Switzerland) with an inlet drying air temperature of 60°C. When the outlet air reached 50°C, drying ended. Drying of spheroids took ~30 minutes.

Characterization of Spheroids

Size and Shape Analysis

The time-sampled spheroids were examined qualitatively under 20× magnification using a stereomicroscope (BX61, Olympus, Tokyo, Japan). Images were captured by a digital color video camera (DXC-390P, Sony, Tokyo, Japan) coupled to the stereomicroscope, using imaging analysis software (Micro Image version 4.5, Media Cybernetics, Silver Spring, MD).

The dried spheroids produced were subdivided using a riffler (PT, Retsch, Germany) into 8 portions. A portion, ~120 g, was sized using a nest of sieves of aperture sizes in a $\sqrt[4]{2}$ progression, ranging from 250 μm to 4.00 mm. A sieve shaker (VS1000, Retsch, Haan, Germany) vibrating at an amplitude of 1 mm for 15 minutes was used. The mean size and size distribution of the spheroids were described using mass median diameter (MMD) and span, respectively.[10]

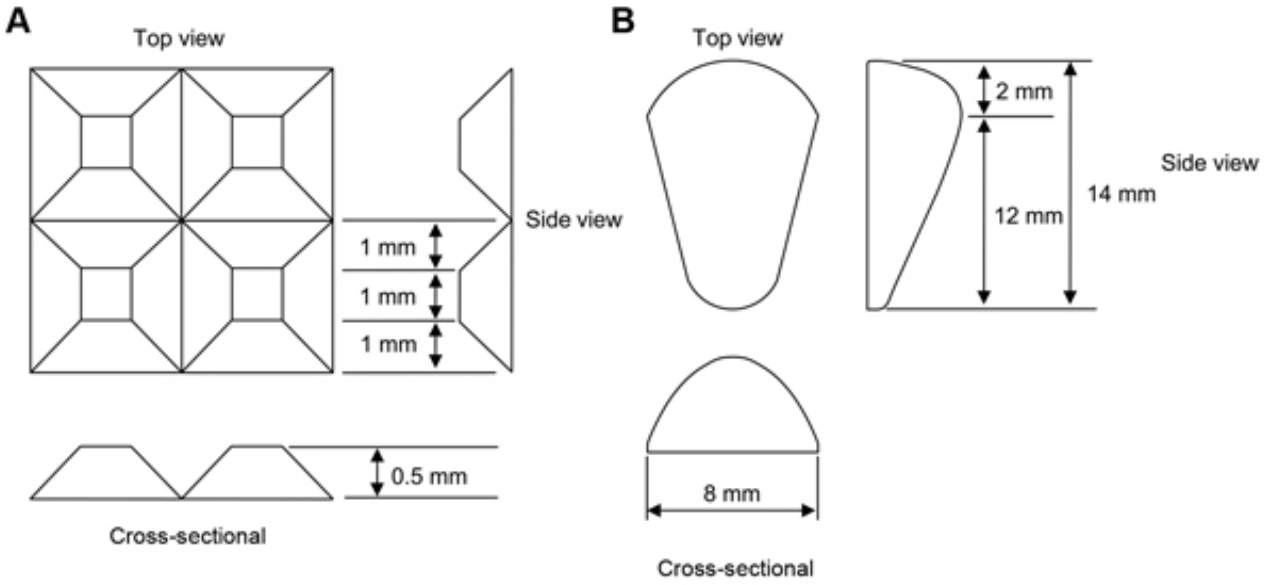

Figure 2. Dimensions of the surface protuberances of (A) cross-hatch and (B) teardrop-studded rotating frictional plates.

Table 2. Process Parameters for ESC and EST batches*

Batch	Speed of Rotation (rpm)	Equivalent Tip Speed (cm·second^{-1})	Gap Air (bar)	Duration of Spheronization (min)
ESC	600	10.1	NA	10
EST793	793	11.4	1.2	20
EST862	862	12.4	1.2	20
EST931	931	13.4	1.2	20
EST1000	1000	14.4	1.2	20

*ESC indicates extrusion-spheronization with cross-hatch plate; EST, extrusion-spheronization with teardrop-studded plate; NA, not applicable.

At least 625 spheroids were randomly sampled from every batch; their images were acquired using a stereomicroscope (SZH, Olympus, Japan) and quantitatively analyzed (System PC-Image Version 2.2.03, Foster Findlay Synoptics, Cambridge, UK). Equivalent circle diameter of spheroids was used to compute the size distribution of spheroids. Roundness of spheroids was quantified using the shape factors: aspect ratio and e_R.[12]

Crushing Strength

Twenty-five randomly chosen spheroids from the 850 to 1000 μm size fraction from each batch were assessed for crushing strength. RT38% was omitted from the test, as it had a negligible amount of spheroids in the specified size fraction. A tensile tester (EZ Test, Shimadzu, Kyoto, Japan) affixed with a platen of diameter 25 mm was used to compress each spheroid at a rate of 3 mm/min. The force required to crush the spheroid was measured by a load cell connected to the platen and recorded using data acquisition software (WinAGS ver 2.01, Kyoto, Japan).

Moisture Content

Approximately 25 g of the MCC:lactose powder mixture was accurately weighed and oven-dried at 70°C to constant weight for quantifying the percentage basal amount of moisture present (W_0). Experiments were in triplicate and results averaged. Likewise, for every batch, ~25 g of spheroids were obtained immediately after processing to be oven-dried at 70°C till constant weight. The percentage total amount of moisture (W_1) in the spheroids was determined. The percentage moisture content of spheroids attributed to the amount of water added was ($W_1 - W_0$).

Table 3. Process Parameters for RT Batches*

Process Parameters	Parameter Values
Equivalent tip speed (cm·second^{-1})	7.2 (first 2 minutes) 13.4 (after 2 minutes)
Gap air (bar)	1.2
Duration of process (min)	20
Inlet air temperature (°C)	30
Atomizing air pressure (bar)	1.2
Spray nozzle diameter (mm)	0.8
Spray rate (g/min)	41

*RT indicates rotary processing with teardrop-studded plate.

Statistical Analysis

The statistical program SPSS version 12.0 was used to carry out all statistical calculations.

Results and Discussion

Average MMD and span values of ESC spheroids were 0.877 mm and 0.283, respectively, indicating that the batches of spheroids produced were of suitable size range and narrowly distributed (Table 4). The batches could be considered a fair representation of good-quality spheroids.

During ESC, the rotating frictional plate achieved a peripheral tip speed of 10.1 cm·second^{-1} (Table 2). Preliminary EST batches were performed at an equivalent tip speed of 10.1 cm.second^{-1} (698 rpm), for 20 minutes. The spheroids produced were, however, smaller and less spherical than those produced by ESC. The difference in surface texture between the rotating frictional plates could have caused the difference. Therefore, the surface texture was further examined.

The amount of frictional force exerted by the rotating frictional plate onto extrudates could be estimated by examining the geometry and the number of protuberances per unit surface area on the rotating frictional plate. Surface protuberances on the cross-hatch plate were sharp-edged and relatively smaller than the teardrop studs on the rotary processor (Figure 2). The surfaces of both plates were visually examined, and calculations revealed that per 10 cm^2, there were 111.1 cross-hatch studs and 6.2 teardrop studs on the respective plates. The rounded edge of the teardrop studs and the lower density of studs per unit area indicated that the amount of frictional force exerted by the teardrop-studded rotating frictional plate would be lower than that of the cross-hatch rotating frictional plate at an equivalent peripheral tip speed of 10.1 cm.second^{-1}. With an identical peripheral tip speed, processes such as size enlargement by coalescence, densification, and rounding of EST extrudates could occur at a comparatively slower rate, resulting in smaller

Table 4. Size, Size Distribution, Roundness, and Moisture Content of Spheroids*

Batch	MMD (mm)	Span	Aspect Ratio	e_R	Moisture (% wt/wt)	Crushing Strength (N)
ESC	0.877 (0.057)	0.283 (0.0374)	1.085 (0.0042)	0.620 (0.0091)	37.71 (0.360)	6.06 (1.429)
EST793	0.767 (0.040)	0.305 (0.0441)	1.106 (0.0048)	0.599 (0.0090)	29.57 (0.375)	4.17 (1.368)
EST862	0.777 (0.006)	0.352 (0.0385)	1.089 (0.0048)	0.631 (0.0117)	28.89 (0.411)	3.95 (1.624)
EST931	0.880 (0.066)	0.267 (0.0362)	1.079 (0.0026)	0.638 (0.0029)	29.00 (0.262)	5.65 (2.720)
EST1000	0.923 (0.067)	0.253 (0.0715)	1.068 (0.0022)	0.654 (0.0054)	28.36 (0.308)	6.24 (2.717)
RT36%	0.940 (0.106)	0.369 (0.0527)	1.135 (0.0250)	0.570 (0.0249)	28.79 (0.476)	11.19 (2.679)
RT37%	1.103 (0.133)	0.302 (0.0130)	1.102 (0.0193)	0.590 (0.0023)	29.85 (0.291)	12.67 (1.803)
RT38%	1.390 (0.210)	0.287 (0.0298)	1.097 (0.0026)	0.609 (0.0015)	31.09 (0.337)	—

*Values are mean (SD). MMD indicates mass median diameter; ESC, extrusion-spheronization with cross-hatch plate; EST, extrusion-spheronization with teardrop-studded plate; RT, rotary processing with teardrop-studded plate.

and less spherical spheroids in a similar time frame. Wan et al[11] showed that with increased spheronization speed and duration, spheroids became bigger and rounder. Thus, for the teardrop-studded frictional surface to exert an overall frictional force comparable to that of the cross-hatch surface, spheronization had to be performed at a higher peripheral tip speed.

Apart from peripheral tip speed, establishing equivalency in the effect of the rotating frictional plates also entails finding an appropriate duration for spheronization. A typical RP production batch would last for 20 minutes, inclusive of the time required for water addition. Comparison between forces experienced by agglomerates during spheronization by the different methods led to the duration of spheronization for EST being set at around 20 minutes.

EST was performed with a higher peripheral tip speed (Table 2) for 20-minute spheronization to empirically elucidate equivalency in the effect of the frictional plate. The average MMD of spheroids produced by EST at 793 to 1000 rpm ranged from 0.767 to 0.923 mm (Table 4). At 931 rpm, EST produced spheroids of average MMD of 0.880 mm, which, in terms of size, was the closest to ESC. EST931's span was also close to ESC's (Table 4). Therefore, in terms of size and size distribution of spheroids produced, ESC and EST931 could be concluded to be equivalent in the spheronization process, indicating that the spheroids were experiencing an equivalent amount of frictional force.

After spheronization process equivalency between ESC and EST was elucidated, spheroids were produced by RP with a rotating plate peripheral tip speed of 13.4 cm.second^{-1} so as to achieve comparable spheronizing conditions as those used by ESC and EST (Table 3).

At equivalent spheronizing conditions and the same amount of moistening liquid, RT38% spheroids were distinctly larger than the ESC and EST931 spheroids (Table 4). As reducing the amount of water can generally reduce the size of spheroids produced by RP,[13] less water was used for wet massing in order to produce spheroids of comparable size to those of ESC and EST. In this study, 360 mL of water was the lowest amount used for the production of spheroids by RP. When the amount of water was decreased to 350 mL, the spheroids produced were very small and accompanied by a large amount of fines, making the spheroid batch unsuitable for this study.

ESC, EST931, and RT36% could be considered to be batches of spheroids with similar size in terms of average MMD (Table 4). Therefore, spheroids produced by ES and RP could be compared objectively as important process and formulation parameters were kept constant or equivalent. Spheroids produced were compared according to the following aspects: size distribution of spheroids, sphericity, and crushing strength.

ESC, EST931, and RT36% spheroids had a similar narrow size distribution. The average span was 0.283 for ESC and 0.253 to 0.352 for EST at the series of peripheral tip speeds investigated. On the other hand, RT36%'s span was 0.369 (Table 4). One-way analysis of variance (ANOVA) indicated no significant difference in span between ESC, EST931, and RT36% spheroids despite an observable trend that indicated that ESC and EST spheroids were more narrowly distributed than those of RT36% (Tables 4 and 5). Using size and shape data gathered from image analysis, we computed descriptors for size distribution, namely mean, SD, skewness, and kurtosis, to critically evaluate for any difference in the size distribution of spheroids produced by ESC, EST931, and RT36% (Table 6). One-way ANOVA and post hoc least squares difference test indicated that RT36% spheroids had wider size distribution, greater positive skewness, and greater kurtosis than ESC or EST931 spheroids (Tables 5 and 6).

Two possibilities might have caused the differences in size distribution: the extrusion process or the teardrop-studded rotating frictional plate. As size distribution was not significantly different between ESC and EST931 (Table 5), it could be postulated that the teardrop-studded rotating frictional plate was unlikely to have caused the differing size distribution of RT36% spheroids. Regardless of their surface design, when the rotating frictional surfaces were in motion, they provided the necessary frictional force for moving and

Table 5. One-Way ANOVA and Post Hoc LSD Test*

Variable Tested	Batch	*P* for 1-Way ANOVA	Batches Compared	*P* for Post Hoc LSD Test
Moisture content	EST793	0.000†	EST793 vs EST862	0.036†
	EST862		EST793 vs EST931	0.069
	EST931		EST793 vs EST1000	0.001†
	EST1000		EST793 vs RT36%	0.019†
	RT36%		EST793 vs RT37%	0.362
	RT37%		EST793 vs RT38%	0.000†
	RT38%		EST862 vs EST931	0.724
			EST862 vs EST1000	0.091
			EST862 vs RT36%	0.745
			EST862 vs RT37%	0.006†
			EST862 vs RT38%	0.000†
			EST931 vs EST1000	0.047†
			EST931 vs RT36%	0.501
			EST931 vs RT37%	0.011†
			EST931 vs RT38%	0.000†
			EST1000 vs RT36%	0.160
			EST1000 vs RT37%	0.000†
			EST1000 vs RT38%	0.000†
			RT36% vs RT37%	0.003†
			RT36% vs RT38%	0.000†
			RT37% vs RT38%	0.001†
Span	ESC	0.714	ESC vs EST931	0.666
	EST931		ESC vs RT36%	0.048†
	RT36%		EST931 vs RT36%	0.026†
Mean	ESC	0.275	ESC vs EST931	0.719
	EST931		ESC vs RT36%	0.138
	RT36%		EST931 vs RT36%	0.231
SD	ESC	0.023†	ESC vs EST931	0.733
	EST931		ESC vs RT36%	0.013†
	RT36%		EST931 vs RT36%	0.020†
Skewness	ESC	0.000†	ESC vs EST931	0.337
	EST931		ESC vs RT36%	0.000†
	RT36%		EST931 vs RT36%	0.001†
Kurtosis	ESC	0.005†	ESC vs EST931	0.838
	EST931		ESC vs RT36%	0.003†
	RT36%		EST931 vs RT36%	0.003†
Aspect ratio	ESC	0.000†	ESC vs EST793	0.035†
	EST793		ESC vs EST862	0.697
	EST862		ESC vs EST931	0.483
	EST931		ESC vs EST1000	0.080
	EST1000		ESC vs RT36%	0.000†
	RT36%		EST793 vs EST862	0.070
			EST793 vs EST931	0.009†
			EST793 vs EST1000	0.001†
			EST793 vs RT36%	0.035†
			EST862 vs EST931	0.284
			EST862 vs EST1000	0.040†
			EST862 vs RT36%	0.000†
			EST931 vs EST1000	0.258
			EST931 vs RT36%	0.000†
			EST1000 vs RT36%	0.000†
e_R	ESC	0.000†	ESC vs EST793	0.066
	EST793		ESC vs EST862	0.309
	EST862		ESC vs EST931	0.104
	EST931		ESC vs EST1000	0.006†

Table 5. Cont.

Variable Tested	Batch	*P* for 1-Way ANOVA	Batches Compared	*P* for Post Hoc LSD Test
	EST1000		ESC vs RT36%	0.000†
	RT36%		EST793 vs EST862	0.009†
			EST793 vs EST931	0.003†
			EST793 vs EST1000	0.000†
			EST793 vs RT36%	0.016†
			EST862 vs EST931	0.500
			EST862 vs EST1000	0.044†
			EST862 vs RT36%	0.000†
			EST931 vs EST1000	0.145
			EST931 vs RT36%	0.000†
			EST1000 vs RT36%	0.000†
Crushing strength	ESC	0.000†	ESC vs EST793	0.000†
	EST793		ESC vs EST862	0.000†
	EST862		ESC vs EST931	0.240
	EST931		ESC vs EST1000	0.600
	EST1000		ESC vs RT36%	0.000†
	RT36%		ESC vs RT37%	0.000†
	RT37%		EST793 vs EST862	0.527
			EST793 vs EST931	0.000†
			EST793 vs EST1000	0.000†
			EST793 vs RT36%	0.000†
			EST793 vs RT37%	0.000†
			EST862 vs EST931	0.000†
			EST862 vs EST1000	0.000†
			EST862 vs RT36%	0.000†
			EST862 vs RT37%	0.000†
			EST931 vs EST1000	0.089
			EST931 vs RT36%	0.000†
			EST931 vs RT37%	0.000†
			EST1000 vs RT36%	0.000†
			EST1000 vs RT37%	0.000†
			RT36% vs RT37%	0.000†

*ANOVA indicates analysis of variance; LSD, least squares difference; EST, extrusion-spheronization with teardrop-studded plate; RT, rotary processing with teardrop-studded plate; ESC, extrusion-spheronization with cross-hatch plate.
†Denotes statistical significance at .05 level.

remodeling the aggregated contents. The resultant spheroid size would be due to a balance of coalescence and breakdown during spheronization.[11] Breakdown of spheroids could be caused by these factors: excessive forces exerted by the frictional surface, intense collision between spheroids, or intense collision between the spheroid and the container wall. Compared with the sharp-edge cross-hatch surface, the teardrop studs with round edges would most likely exert lower breakdown forces. The apparent similarity in size distributions of ESC and EST931 spheroids indicated that the degree of agglomeration and breakdown of spheroids would be determined by the collisions encountered by the spheroids and not the nature of the rotating frictional plate surface.

The different spheroid formation mechanisms by ES and RP would cause differences in the shape of the size distributions of spheroids produced by ESC and RT. Two studies have reported that the proportion of unicored and multicored microcapsules could be revealed by analyzing the bimodal size distribution,[14] and the size distribution of crushed materials could be represented by Rosin-Rammler distribution.[15] Through analysis of the size distributions of multiparticulate systems, therefore, underlying formative processes could be revealed. When the 2 processes were compared, size distributions of ESC and EST931 spheroids were significantly more symmetrical and more narrowly distributed than those of RT36% spheroids (Tables 5 and 6). Size analysis using sieves indicated that 3.36% by weight of RT36% spheroids were larger than 1.7 mm. The proportion of ESC and EST931 spheroids larger than 1.7 mm (≤0.06%) was negligible. The oversized spheroids present in RT36% contributed to the positive skewness and higher kurtosis. The extrusion step in ES could have prevented the occurrence of such lumps. ES and RP spheroid formation mechanisms were further investigated.

Table 6. Statistical Descriptors for Size Distribution of Spheroids

Statistical Descriptors	Batch		
	ESC	EST931	RT36%
Mean	993.1	1086	1193
	1079	951.1	986.5
	940.5	1065	1241
SD	107.0	87.8	189.4
	89.4	161.8	169.3
	124.2	94.3	191.1
Skewness	0.567	1.135	2.807
	0.860	1.022	3.518
	0.580	1.007	4.333
Kurtosis	–0.131	2.766	14.68
	1.753	0.527	27.46
	–0.473	1.285	37.00

*ESC indicates extrusion-spheronization with cross-hatch plate; EST, extrusion-spheronization with teardrop-studded plate; RT, rotary processing with teardrop-studded plate.

Visual examination of time-sampled spheroids under an optical microscope revealed significant differences in the spheroid formation mechanism for both processes. Images that depict significant changes during spheroid formation appear in Figure 3.

The general morphological changes of spheroids during spheronization for ESC and EST931 were similar (Figure 3). Cylindrically shaped extrudates were visually examined to have an average length of ~5 to 10 mm. Spheronization began with the rapid breakdown of extrudates by attrition around the edges and fractures across the extrudates caused by the impact of the textured rotating frictional plate and collisions between extrudates and the container wall. Extrudates were broken within 0.5 minutes into 2 distinct populations, aggregates of size ~1 mm and 0.2 mm in length. The larger aggregates were termed core aggregates and the smaller aggregates were termed fines. At 1 minute into spheronization, fines that initially appeared to be irregularly shaped became rounder and slightly larger. These fines increased in size by coalescence between fines. Aggregates that were larger than fines but smaller than core aggregates were termed nucleated aggregates. As spheronization proceeded into the second minute, these nucleated aggregates became increasingly round and large concurrently with the core aggregates. Beyond the second minute, the amount of unagglomerated individual particles reduced considerably and the remaining population consisted of only nucleated aggregates and core aggregates. These had also grown rounder. The disparity in size between the nucleated aggregates and core aggregates was small compared with the difference between the fines and the core aggregates. The nucleated aggregates became progressively larger with time, while the core aggregates remained largely unchanged in size. From the fourth minute onward, core aggregates and nucleated aggregates were indistinguishable from one another and aggregates became uniform in size.

High-speed video footage of spheronization for ESC revealed images that were in agreement with observations made on

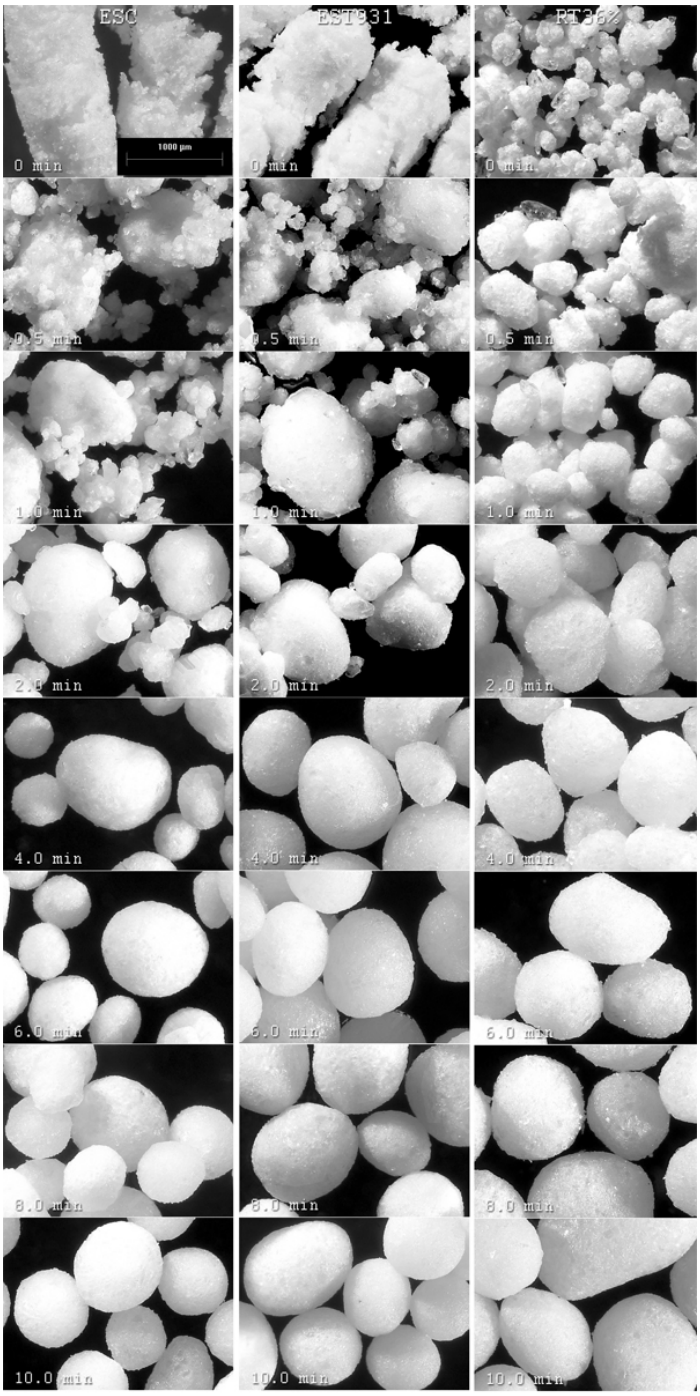

Figure 3. Stages of spheroid formation in ESC, EST931, and RT36%. For ESC and EST931, time annotations indicate time lapsed during spheronization. For RT36%, time annotations indicate time lapsed after completion of water addition. ESC indicates extrusion-spheronization with cross-hatch plate; EST, extrusion-spheronization with teardrop-studded plate; RT, rotary processing with teardrop-studded plate.

time-sampled spheroids of ESC (Figure 4). At 0.5 minutes into spheronization, the population consisted of less spherical core aggregates that had many fines attached to their surfaces. Core aggregates were more spherical, and nucleated aggregates were observed at 1 minute into spheronization. With consolidation, core aggregates became resistant to growth but progressively became rounder, while nucleated aggregates continued to grow bigger and rounder as the spheronization run progressed (Figure 4).

Without the extrusion stage, the formation of RT36% spheroids was different. Upon completion of the water addition, the aggregates were observed (Figure 3). Unlike the ESC and EST931 aggregates, the RT36% aggregates did not exhibit a bimodal size distribution at 0.5 minutes upon completion of the water addition. Instead, the size of aggregates ranged from 300 to 800 μm. The variability in aggregate size decreased considerably after 0.5 minutes. At 1.5 minutes and beyond, the size of agglomerates ceased to increase, and they became rounder.

The morphological changes revealed differences in spheroid formation between ES and RP. In general, spheroid production is considered to be a specialized form of granulation. The classic granulation model depicts 3 stages: wetting and nucleation, consolidation and growth, and attrition and breakdown.[16] In ES, nucleation of particles occurred when the powder mix was moistened. Agglomerates formed experienced compressive forces during transit through the extrusion screen, resulting in consolidation and formation of extrudates. Nucleation occurred in RP in a similar manner when water was sprayed onto the powder. Consolidation of nuclei was brought about by the shearing forces of the rotating frictional plate. However, excessive shear forces caused breakdown of agglomerates.

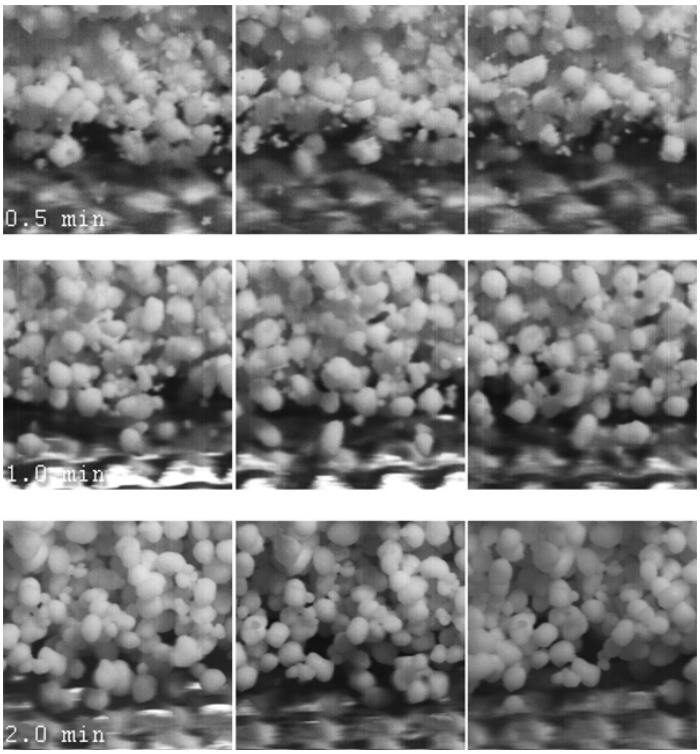

Figure 4. Sequential frames of spheroid formation captured in situ using high-speed video camera. Time annotations indicate time lapsed during spheronization.

During spheronization, extrudates were fractured across their lengths (by shear forces from the rotating frictional plate surface, collision among extrudates, or collision between extrudates and container wall), yielding the core aggregates. Edges and surface irregularities of the extrudates underwent attritions, yielding fines. The occurrence of core aggregates and fines resulted in a characteristic bimodal size distribution shown in Figure 3 for the 0.5- and 1-minute samples of ESC and EST931. The initial phase of breakdown was followed by size enlargement by these mechanisms: coalescence of fines forming aggregates, coalescence of aggregates with core aggregates, and layering of fines onto core aggregates. A model proposed by Rowe[2] suggested that extrudates were rounded at the edges and then dumbbell-shaped aggregates were formed. These dumbbell-shaped aggregates were intermediates that proceeded to become elliptical spheres, eventually rounding to yield spheroids. This model suggested that extrudates were relatively plastic, nonbrittle, and able to deform during spheronization to form dumbbells. The alternative model proposed by Baert and Remon[4] also involved the formation of dumbbells as intermediates. However, the differing aspect was that the dumbbell would break into 2 in the middle. Folding would occur at the point of breakage before spheroids eventually formed. Dumbbell-shaped intermediates, if formed, would likely be observed at the beginning of spheronization (0-2 minutes). Visual observation of spheroid formation for ESC and EST931, however, indicated that the formation of dumbbell-shaped intermediates was unlikely unless they were formed within the first 30 seconds of spheronization. High-speed video footage revealed the existence of elongated core aggregates (Figure 4). However, these elongated core aggregates did not appear as dumbbell precursors but as short, rodlike core aggregates. These core aggregates progressively became rounder without a distinct decrease in size in the midsection, as would be evident in the event of dumbbell breakage. Dumbbell breakage and folding was hypothesized to account for the presence of cavities within spheroids.[2,7] Pisek et al[7] produced spheroids by ES and RP with varying amounts of lactose and noticed that higher percentages of lactose in the formulation correlated with larger cavities within the spheroids, indicating the possibility that the cavities would likely be present if the spheroid formulation contained soluble excipients. Remodeling also tended to be more of a surface phenomenon, with the cohesive but plastic aggregate surfaces remodeled or realigned

along the circumferential direction, away from the ends of the longer axes, to the midsections, as the impact forces were regular but of low magnitudes. Entrapped cavities would likely remain unaffected as the impact forces were dissipated along the agglomerate surfaces as they remodeled. In fact, the remodeling process itself could have contributed to the existence or enlargement of entrapped cavities. As the rodlike aggregate ends were pressured inward by impact forces, the midsection might have been forced outward by inward-moving water liberated by the spongelike microcrystalline particles,[17] contributing to high water pressure within. Subsequently, these water-rich regions dried and became cavities in the pellets. This observation provided an alternative explanation for the existence of the cavities, complementing the observations by other investigators discussed earlier. Although the spheroid formation mechanism could be different using different formulation or process parameters, within the limits of this study, in which the formulation used was able to produce typically good-quality spheroids of suitable size and narrow size distribution, the ES spheroid formation mechanism could be described as follows:

1. breakdown of extrudates to lengths approximately equal to their diameter,
2. attrition of corners and edges of extrudates, producing core aggregates and fines,
3. layering of fines onto core aggregates, coalescence between fines and small aggregates to form larger core aggregates, and
4. remodeling of rodlike aggregates by gradual and consistent impacts on the circumferential edges to form spheroids of high sphericity (Figure 5A).

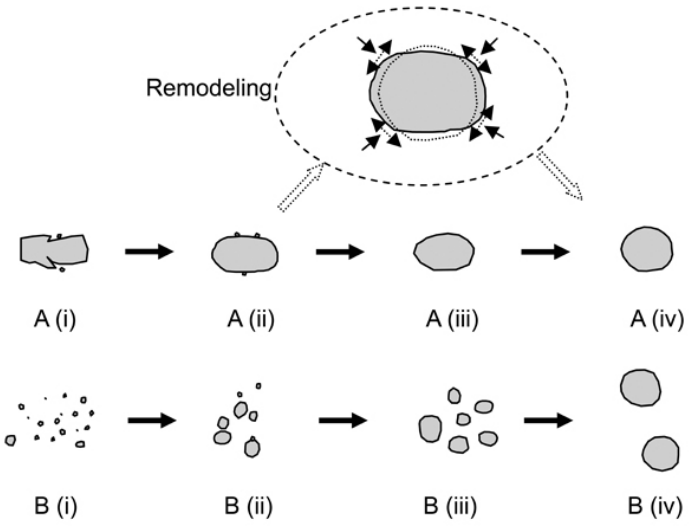

Figure 5. Model of spheroid formation by (A) extrusion-spheronization and (B) rotary processing.

By comparison, the RP spheroid formation mechanism follows this pattern:

1. nuclei formation from agglomeration of wetted particles,
2. agglomeration of nuclei, forming small agglomerates,
3. layering of fines onto larger agglomerates, and
4. coalescence of agglomerates and rounding to form spheroids (Figure 5B).

The observed differences in spheroid formation and presence of lumps for RT36% indicated the importance of uniform water distribution in RP. A homogenous distribution of water within the powder mix depended on factors such as movement of the powder mix and spray rate. Powder movement was in turn influenced by its rheology and the speed of the rotating frictional plate. When powder did not flow uniformly or consistently, its transit time and passage across the spray zone became irregular, resulting in localized overwetting. In a high-shear mixer granulator, an increase in the amount of granulating liquid would increase the rate of granule growth and the resultant size of the granules.[18] Relating this to a rotary processor, localized overwetting caused rapid agglomerate growth, bringing about a disparity in sizes of formed agglomerates in the processor. For coalescence of nondeformable granules, the opportunity to coalesce upon impact was higher between granules of dissimilar sizes.[16] The opportunity to coalesce between granules of similar sizes would be inversely proportional to their sizes. Therefore, this model postulated that there exists a maximum size that granules can achieve by coalescence. During spheronization, large aggregates increased in size by a "snowball effect," continuing to coalesce smaller aggregates. Aggregate size would reach a maximum when the amount of moisture on the surface was insufficient to facilitate subsequent successful coalescence. Excessively large aggregates would also be broken down by the impact forces exerted by the textured surface of the frictional rotating plate. The negligible amount of spheroids larger than 1.7 mm in ESC and EST931 spheroid batches suggested that the extrudates were uniformly wetted. The separate moistening step of mixing with an impeller and the extrusion step had effectively ensured a uniformly wetted mass for spheronization. In addition, as the spheronization process progressed, there was concurrent loss of moisture by evaporation. This also acted as a barrier to agglomerate growth with time. In fact, if spheronization was extended beyond the usual run time for making good spheroids, breakdown of formed spheroids would have occurred.

Generally, the amount of water remaining in spheroids after spheronization need not always correlate with the final spheroid size. In this study, spheroids of equivalent size could be produced using RP with less water than ESC and EST931 required. However, in another study,[7] RP used more water

than ES to produce similar spheroids. In their RP studies, Vertommen et al[19] attributed the differences in spheroid size to the amount of water remaining after accounting for moisture loss by the gap and atomizing air. The moisture content of RT38% spheroids was 31.09% wt/wt and decreased by ~1.1% wt/wt consistently from RT38% to RT36% (Table 4). Although equal amounts of granulating liquid were used for EST and RT38%, the moisture content of RT38% spheroids was higher than that of EST spheroids. Exposure of extrudates to the gap air resulted in faster moisture loss. This could be attributed to better air flow through the extrudates than through the wetted powder mass. Another possibility would be that during extrusion, water might have migrated to extrudate surfaces, leading to a greater amount of moisture being lost during spheronization. The fact that the size of spheroids from RT36%, EST862, EST931, and EST1000 was comparable seemed to indicate that the amount of moisture remaining in the spheroids upon spheronization could determine the final spheroid size. However, RT37% and EST793 spheroid sizes differed widely despite having a similar amount of moisture; thus, the final amount of water remaining in the spheroids could not be a reliable predictor of the final size of spheroids produced using different processes. Comparing ESC and EST spheroids, EST spheroids experienced significant moisture loss due to the gap air. The average moisture content of spheroids produced by EST ranged from 29.6% to 28.4% wt/wt, and increasing the speed of the rotating frictional plate caused greater water loss. Despite the differences in moisture remaining in the spheroids, ESC and EST batches of spheroids had similar sizes. This indicated that the quantity of moisture lost during spheronization would not have a major effect on the eventual spheroid size for multistep ESC and EST as the process of spheroid formation reached almost the final size within a minute into the spheronization run. Subsequent moisture loss would have minimal effect unless the integrity of the spheroids was compromised.

The choice of peripheral tip speed, duration, and protuberance on the rotating frictional plate did not significantly affect the roundness of spheroids. ESC did not produce rounder spheroids compared with EST ($P > .05$) (Tables 4 and 5). The similarity in roundness and size of ESC and EST spheroids further reinforced the possibility that spheroid formation relied mainly on collision between spheroids and less on collision between the well-defined textured surface of the rotating frictional plate and spheroids. In this study, aspect ratio and e_R indicated increasing roundness with higher peripheral tip speed for EST spheroids, similarly observed by Wan et al[11] and Newton et al.[20]

RT36% spheroids were significantly less spherical than ESC or EST spheroids (Table 4 and 5). During spheronization, aggregates have to possess a balance of rigidity and plasticity in order to be rounded into spheroids of the desired size. RT36% spheroids, having comparatively less water than ESC and EST spheroids, were more rigid, less deformable, and consequently less round. With an increased amount of water, the roundness of RT spheroids was improved. However, the consequential increase in plasticity due to the higher amount of water also yielded larger spheroids, which became unsuitable for equivalent size comparison with those of ESC.[21]

At equivalent spheronizing conditions, the ESC, EST931, and EST1000 spheroids produced had a similar crushing strength (Table 5). This apparent similarity in crushing strength, size, and size distribution between ESC and EST931 spheroids further reinforced the possibility that the spheroid formation process would be more influenced by spheroid-spheroid collisions than by spheroid–plate surface collisions. Although EST931 spheroids experienced greater moisture loss during spheronization, spheroid integrity remained similar to that of ESC spheroids and rather similar crushing strength was obtained. Mean crushing strength of EST spheroids increased with increasing spheronization speed. This indicated that greater densification forces were experienced by spheroids during spheronization as spheroids collided more forcefully with one another or with the wall of the container at higher disc rotation speeds. However, the increase in crushing strength of spheroids with higher spheronization speed was not observed by Kleinebudde et al.[22] RT37% spheroids had a higher crushing strength than did those of RT36%. Pore volumes were reported to reduce when greater amounts of water were used.[23] A greater amount of water could have increased the percentage of lactose dissolved, thus allowing more extensive solid bridges to be formed upon drying. In this study, RT36% spheroids had significantly higher crushing strengths than did spheroids produced by ESC or EST. In contrast, Pisek et al[7] reported that spheroids produced by RP were more friable compared with those produced by ES, while Robinson and Hollenbeck[8] could not find a significant difference in crushing strength between spheroids produced by RP and ES. Two possible factors could have caused the differences in spheroid crushing strength: (1) differences in the amounts of water used, and/or (2) differences in the spheroid-forming process. Given that, as mentioned above, a greater amount of water would reduce the pore volume of the spheroid matrix, it would be unlikely that ESC or EST spheroids would be weaker. With extrusion, ES spheroids were formed differently than RP spheroids were. The occurrence of core aggregates and layering of fines during the initial stage of spheronization produced aggregates with a less homogenous matrix in terms of particle-particle arrangements. During RP, nuclei formation, agglomeration of nuclei, and coalescence of aggregates with the possibility of minimal layering of fines produced better-consolidated aggregates with higher crushing strengths.

CONCLUSION

In ES, extrudates spheronized with dissimilar frictional plates could achieve similar roundness, mean size, and size distribution when appropriate peripheral tip speed and duration were used. Compared with the size distribution of ES spheroids, the size distribution of RP spheroids had a greater SD, greater positive skewness, and greater kurtosis. ES spheroids showed evidence of attrition and layering, unlike RP spheroids, where nucleation and agglomeration were more predominant. Without the extrusion process, RP could produce spheroids with a higher crushing strength than those of ES.

REFERENCES

1. Sellassie IG. Pellets: a general overview. In: Sellassie IG, ed. *Pharmaceutical Pelletization Technology.* New York, NY: Marcel Dekker; 1989:1–13.

2. Vervaet C, Baert L, Remon JP. Extrusion-spheronization, a literature review. *Int J Pharm.* 1995;116:131–146.

3. O'Conner RE, Schwartz JB. Extrusion and spheronization technology. In: Sellassie IG, ed. *Pharmaceutical Pelletization Technology.* New York, NY: Marcel Dekker; 1989:187–216.

4. Baert L, Remon JP. Influence of amount of granulation liquid on the drug release rate from pellets made by extrusion spheronization. *Int J Pharm.* 1993;95:135–146.

5. Fielden KE, Newton JM, Rowe RC. The influence of lactose particle size on spheronization of extrudate processed by a ram extruder. *Int J Pharm.* 1992;81:205–224.

6. Liew CV, Wan LSC, Heng PWS. Influence of polytetrafluoroethylene on spheroid production by rotary processing. *STP Pharma Sci.* 1998; 8:297–302.

7. Pisek R, Sirca J, Svanjak G, Sricic S. Comparison of rotor direct pelletization (fluid bed) and extrusion/spheronization method for pellet production. *Pharm Ind.* 2001;63:1202–1209.

8. Robinson RL, Hollenbeck RG. Manufacture of spherical acetaminophen pellets: comparison of rotary processing with multiple-step extrusion and spheronization. *Pharm Technol.* 1991;15:48–56.

9. Newton JM, Chapman SR, Rowe RC. The influence of process variables on the preparation and properties of spherical granules by process of extrusion and spheronization. *Int J Pharm.* 1995;120:101–109.

10. Heng PWS, Liew CV, Gu L. Influence of teardrop studs on the rotating frictional base plate on spheroid quality in rotary spheronization. *Int J Pharm.* 2002;241:173–184.

11. Wan LSC, Heng PWS, Liew CV. Spheronization conditions on spheroid shape and size. *Int J Pharm.* 1993;96:59–65.

12. Podczeck F, Rahman SR, Newton JM. Evaluation of a standardized procedure to assess the shape of pellets using image analysis. *Int J Pharm.* 1999;192:123–138.

13. Heng PWS, Wan LSC, Tan YTF. Optimization of spheroid production by centrifugal rotary processing. *Int J Pharm.* 1996;143:107–112.

14. Morris NJ, Warburton B. Particle size analysis of microcapsules. *J Pharm Pharmacol.* 1984;36:73–76.

15. Wanibe Y, Itoh T. Distribution of particle sizes. In: Wanibe Y, Itoh T, eds. *New Quantitative Approach to Powder Technology.* New York, NY: John Wiley & Sons; 1998:29–47.

16. Iveson SM, Litster JD, Hapgood K, Ennis BJ. Nucleation, growth and breakdown phenomena in agitated wet granulation processes: a review. *Powder Technol.* 2001;117:3–39.

17. Heng PWS, Koo OMY. A study of the effects of the physical characteristics of microcrystalline cellulose on performance in extrusion spheronization. *Pharm Res.* 2001;18:480–487.

18. Hoornaert F, Wauters PAL, Meesters GMH, Pratsinis SE, Scarlett B. Agglomeration behaviour of powders in a Lödige mixer granulator. *Powder Technol.* 1998;96:116–128.

19. Vertommen J, Rombaut P, Michoel A, Kinget R. Estimation of the amount of water removed by gap and atomization air streams during pelletization in a rotary processor. *Pharm Dev Technol.* 1998;3:63–72.

20. Newton JM, Chapman SR, Rowe RC. The assessment of the scale-up performance of the extrusion/spheronisation process. *Int J Pharm.* 1995;120:95–99.

21. Harris MR, Sellassie IG. Formulation variables. In: Sellassie IG, ed. *Pharmaceutical Pelletization Technology.* New York, NY: Marcel Dekker; 1989:217–239.

22. Kleinebudde P, Schroder M, Schultz P, Muller BW, Waaler T, Nymo L. Importance of the fraction of microcrystalline cellulose and spheronization speed on the properties of extruded pellets made from binary mixtures. *Pharm Dev Technol.* 1999;4: 397–404.

23. Vertommen J, Rombaut P, Kinget R. Internal and external structure of pellets made in a rotary processor. *Int J Pharm.* 1998;161: 225–236.